Ultrafast Formation of a Fermi-Dirac Distributed Electron Gas

G. Rohde,[*] A. Stange, A. Müller, M. Behrendt, L.-P. Oloff, K. Hanff, T. J. Albert,
P. Hein, K. Rossnagel, and M. Bauer

Institut für Experimentelle und Angewandte Physik, Christian-Albrechts-Universität zu Kiel, 24098 Kiel, Germany

Time- and angle-resolved photoelectron spectroscopy with 13 fs temporal resolution is used to follow the different stages in the formation of a Fermi-Dirac distributed electron gas in graphite after absorption of an intense 7 fs laser pulse. Within the first 50 fs after excitation, a sequence of time frames is resolved that are characterized by different energy and momentum exchange processes among the involved photonic, electronic, and phononic degrees of freedom. The results reveal experimentally the complexity of the transition from a nascent nonthermal towards a thermal electron distribution due to the different timescales associated with the involved interaction processes.

The extraordinary nonlinearities and optical response times of graphitic materials suggest useful applications in photonics and electronics, including light harvesting [1,2], ultrafast photodetection [3,4], terahertz lasing [5,6], and saturable absorption [7,8]. Both characteristics are closely linked to the ultrafast dynamics of photoexcited carriers, which for this material class is governed by weakly screened carrier-carrier scattering and carrier-phonon interaction. Fundamental aspects related to these processes were addressed in different time-domain studies in the past [9–13]. Because of limitations in the time resolution, most of these studies were restricted, however, to the characteristic timescales of electron-lattice equilibration, i.e., timescales ranging from ≈ 100 fs to ≈ 10 ps.

The primary processes directly after photoexcitation are, in contrast, still largely unexplored and were investigated experimentally only in a few studies so far [14–16]. The dynamics in this strongly nonthermal regime is determined by phenomena such as transient population inversion, carrier multiplication, and Auger recombination, but also phonon-mediated carrier redistribution [17–20]. The challenge is to decode the relative importance and temporal sequence of these processes that drive the electronic system from a nascent nonthermal distribution as generated by photoexcitation towards a Fermi-Dirac (FD) distribution within only ≈ 50 fs [14,15]. It is obvious that such investigations rely on experiments capable of sampling this time window at an adequate time resolution on the order of 10 fs, as well as high energy and momentum resolution.

This Letter reports on the nonthermal carrier dynamics in highly oriented pyrolytic graphite (HOPG) as probed in a time- and angle-resolved photoemission spectroscopy (trARPES) experiment that is operated near the transform limit at a resolution of 13 fs (FWHM of the pump-probe cross correlation) [21]. Over the first 100 fs, we monitor the different stages in the temporal evolution of an initially nonthermal carrier distribution generated by the absorption of a 7 fs near-infrared pulse. We are able to dissect the nonthermal to thermal transition into substages, which are characterized by different energy and momentum exchange and redistribution processes among the involved photonic, electronic, and phononic degrees of freedom. Specifically, the experimental data reveal that the initiating photoabsorption process is first followed by momentum redistribution of the excited carriers before effective cooling of the nonthermal carrier distribution due to emission of phonons sets in. An internally thermalized hot electron gas is finally formed after ≈ 50 fs, which on much longer timescales equilibrates with the lattice [22,23]. The results show experimentally that, on the extremely short nonthermal time frame of a few 10 fs, carrier thermalization can be a complex multistep process owing to different timescales and efficiencies associated with momentum and energy relaxation.

Bulk samples of HOPG (Goodfellow, Ltd.) were mechanically cleaved under high vacuum (1×10^{-7} mbar) right before the experiments. TrARPES was performed under ultrahigh vacuum conditions (3×10^{-10} mbar) in a pump-probe configuration [Fig. 1(b)] using 7 fs white light (WL) pump pulses (800 nm center wavelength, 232 nm rms spectral width) and 11 fs extreme ultraviolet (XUV) probe pulses (22.1 eV), both generated by the output of an 8 kHz Ti:sapphire multipass amplifier. Photoelectron spectra were recorded with a hemispherical electron analyzer at an energy resolution of 240 meV. The relative orientation of the HOPG sample and analyzer entrance slit chosen for the experiments resulted in a momentum cut centered at the H point, as indicated by the black line in Fig. 1(c). Experiments were performed at near-normal incidence at two different incident pump fluences of $F = 0.9$ and $F = 1.7$ mJ/cm^2. The pump-pulse polarization was oriented perpendicular to the
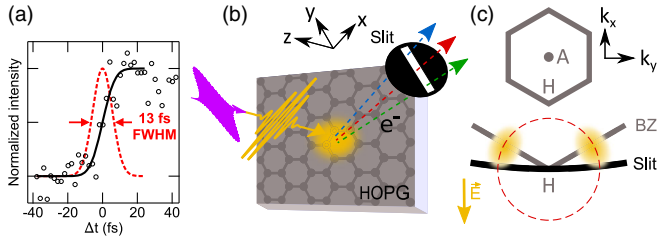
FIG. 1. (a) WL-pump and XUV-probe cross-correlation signal of the experiment. For details see Refs. [21,24]. (b) Schematic of time-resolved pump-probe ARPES of HOPG. Pump pulses are polarized along the x direction. The entrance slit of the electron analyzer is aligned along the y direction. (c) Top: illustration of the Brillouin zone of HOPG. Bottom: closeup of the Brillouin zone (BZ) around the H point (gray) with the momentum cut probed in the experiment indicated (black). The red dashed line marks the constant-energy contour of the π^* band near $E - E_F = 0.8$ eV. Areas of primary excitation are highlighted in yellow.

momentum cut probed in photoemission, as illustrated in Fig. 1(c). The FWHM of the cross correlation signal measured at the sample position yields a value of 13 fs [see Fig. 1(a)] corresponding to a time resolution of 8 fs (5.5 fs), based on a definition introduced in Ref. [16] (Ref. [26]). All data were recorded at an equilibrium sample temperature of 300 K. Further details of the experimental setup are described in Ref. [21].

Figure 2(a) shows trARPES data of HOPG in the vicinity of the H point and around the Fermi energy E_F with the pump-probe time delay set to $\Delta t = -80$ fs, i.e., prior to the excitation by the 7 fs white light pump pulse. The occupied and downward-dispersing π band of HOPG, which at H exhibits an almost linear dispersion [27,28], is well resolved. No indications of the upward-dispersing π^* band are visible, as expected for an undoped sample at thermal equilibrium. Figures 2(b)–2(d) show trARPES data recorded at a pump fluence of 1.7 mJ/cm^2 for selected time delays $0 \leq \Delta t \leq 50$ fs. Distinct changes in the excited state electron distribution taking place on a sub-10 fs timescale are clearly resolved in the experimental data. They become even more evident in a semilogarithmic energy distribution curve (EDC) representation obtained by momentum integration of the raw data following a data analysis scheme described in Ref. [13]. Figures 2(f)–2(h) display the EDC intensities I as a function of energy E for the different time delays after excitation in comparison to the equilibrium state distribution at $T = 300$ K ($\Delta t = -80$ fs). The initial equilibrium state EDC as well as the EDC for $\Delta t = 50$ fs are well described by a FD distribution (see gray dashed lines). In contrast, the data recorded at time zero and at $\Delta t = 13$ fs show clear deviations from a FD distributed population, indicating the strong nonthermal character of the electronic system on sub-50 fs timescales [29].

To evaluate the thermal character of the electron gas at a given time delay, two different quantities are separately
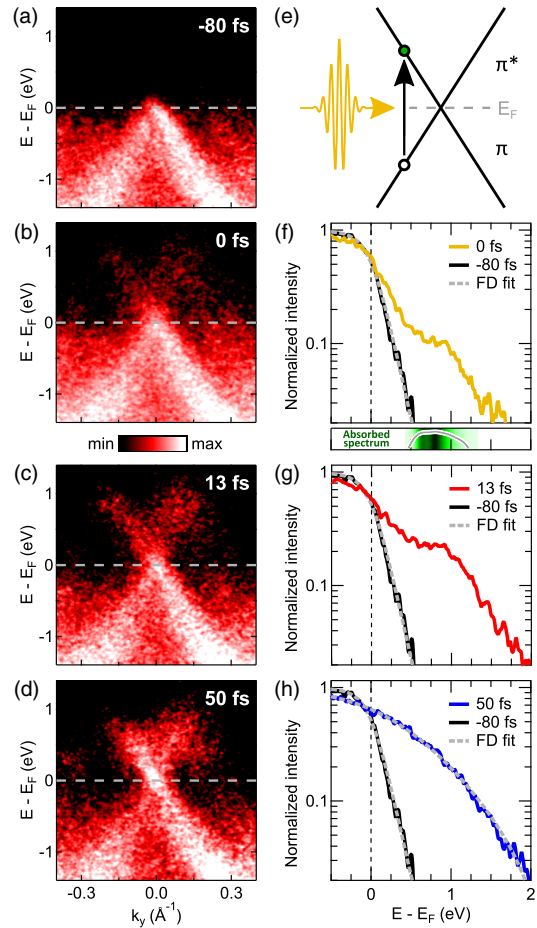

FIG. 2. Time-resolved ARPES data of HOPG taken near H for excitation with 7 fs pump pulses ($F = 1.7$ mJ/cm^2). (a)–(d) ARPES snapshots recorded at different time delays Δt. (e) Illustration of the photoexcitation process. (f)–(h) EDCs around E_F for different Δt derived from the trARPES data. Photoemission intensity was integrated over a momentum window of 0.8 Å^{-1}. Dashed lines are fits of a FD distribution to the EDCs. The inset underneath (f) indicates the pump-pulse spectrum (logarithmic scale) convolved with the energy resolution of the trARPES experiment and mapped onto the energy axis according to the excitation process illustrated in (e). Momentum-resolved photoemission intensity transients are for reference added to the Supplemental Material [24].

extracted from each measured EDC. First, we determine the best-fit Fermi-Dirac temperature T_{FD} [30] from a fit of a FD distribution to the data. Second, we numerically compute the integral

$$E_{\pi^*} = \int_{E > E_F} I(E)E \, dE, \tag{1}$$

being a measure for the total energy stored in the π^* band along the probed momentum cut. Figure 3(a) depicts the relation between E_{π^*} and T_{FD} as it evolves in time in comparison to what is expected for a FD distributed
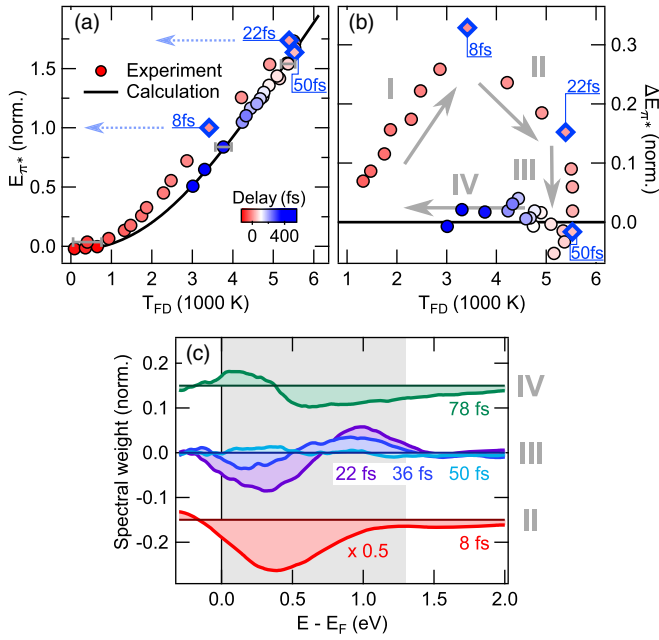
FIG. 3. Analysis of trARPES data for $F = 1.7$ mJ/cm^2. (a) E_{π^*} as a function of T_{FD}. Time markers (blue diamonds) separate the different stages of thermalization identified in (b). Data are normalized to E_{π^*} for $\Delta t = 8$ fs. Error bars indicate exemplary uncertainties in T_{FD}. The solid line is a result of a calculation for a FD distributed electron gas. (b) ΔE_{π^*} as a function of T_{FD}. Arrows indicate the direction of time evolution and different stages in the thermalization process. Similar results for $F = 0.9$ mJ/cm^2 are compiled in the Supplemental Material [24]. (c) Spectrally resolved evolution of the π^* band occupations before, during, and after stage III: difference between experimental EDCs and a FD distributed electron gas for $T = 5500$ K. Data sets and zero lines are partly offset for clarity. Data for $\Delta t = 8$ fs are scaled by a factor of 0.5. Experimental EDCs including fits are for reference added to the Supplemental Material [24].

electron gas (solid line). The color coding of the experimental data indicates the time delay Δt of the measurement, with red corresponding to small delays and blue corresponding to long delays. We consider the measured electron distribution being internally thermalized if the data points lie on top of the result for a FD distribution. The representation of the experimental data in Fig. 3(a) matches the expectation for the buildup and decay of a nonthermal electron distribution following an intense photoexcitation: In response to the absorption of the pump pulse, E_{π^*} starts to increase around time zero and at the same time the data points leave the thermalized regime. Eventually the gain in E_{π^*} stops, and finally, at an equilibrium temperature of ≈ 5500 K, the experimental data points merge into the thermalized regime again. For longer timescales, the electronic system stays internally thermalized and cools down due to coupling to the lattice. The different stages of the nonthermal to thermal transition become more evident in the representation of the data shown in Fig. 3(b). The graph displays the difference ΔE_{π^*} between experimental

results and FD distribution as a function of T_{FD}. ΔE_{π^*} may be considered as a measure of the nonthermal component of E_{π^*}. The distinct changes observable in the slope of ΔE_{π^*} vs T_{FD} suggest the discrimination of four different stages of the thermalization process [labeled I–IV in Fig. 3(b)]. Time markers separating these stages (blue diamonds) are for comparison also added to the data in Fig. 3(a).

The first stage of the probed thermalization process (I) reflects the primary energy input into the electronic system directly resulting from the absorption of the pump pulse. Up to a time delay of $\Delta t \approx 8$ fs, we observe a continuous increase of ΔE_{π^*}, i.e., a continuous buildup of the nonthermal character of the electron gas. This timescale agrees well with the result of an evaluation for the temporal evolution of the absorbed pump-pulse energy under consideration of the experimental parameters: at $\Delta t = 8$ fs the experiment probes a state of the electronic system, where already 93% of the total pump excitation energy has been absorbed.

The second stage of the thermalization process (II) lasts until $\Delta t \approx 22$ fs and is characterized by a continuous decrease of ΔE_{π^*} [see Fig. 3(b)], while T_{FD} as well as E_{π^*} still increase [see Fig. 3(a)]. In the following, we will argue how these observations are related to electron-electron and electron-phonon scattering processes, respectively. The overall detected energy input within stage II corresponds to $\approx 75\%$ of the energy that has been accumulated during the direct absorption process within the first stage [cf. arrows in Fig. 3(a)]. On these intermediate timescales, the photoexcited electron system itself is the only reservoir that can account for a substantial energy gain in the probed region of energy-momentum space. It is result of a carrier redistribution process that is driven by the primary momentum anisotropy generated in graphite upon photoexcitation with linearly polarized light [31,32]. For the pump-pulse polarization used in the present study, the situation is schematically illustrated in Fig. 1(c). Primary population maxima are generated at the intersection of the π^* cone and Brillouin zone boundary (yellow marked areas) and outside of the momentum cut probed in the experiment [31]. The observed secondary gain in E_{π^*} results from a net population transfer out of these primary areas by scattering processes involving a finite azimuthal momentum transfer component, i.e., noncollinear scattering processes [33]. On the relevant timescales and for the pump fluences used in the experiment, noncollinear scattering processes are predominantly due to the interaction of the electrons with strongly coupled optical phonons (SCOPs) [34–36]. The time frame for the decay of the pump-induced momentum anisotropy as implied by our data matches well findings for graphene: results of calculations show that, for pump fluences in the 1 mJ/cm^2 range, an isotropic momentum distribution is formed well within the first 50 fs after excitation [36]. Polarization-dependent photoluminescence measurements performed at

excitation fluences of ≈ 100 μJ/cm^2 hint to a characteristic timescale for this process of ≈ 12 fs [37].

The continuous decrease of the nonthermal character of the electron gas during the second stage as implied by the decrease of ΔE_{π^*} indicates that, simultaneously with the phonon-driven decay of the momentum anisotropy, the energy distribution of the electrons starts to converge towards a FD distribution. In the pump fluence regime of our experiment, this process is dominated by collinear scattering processes due to Coulomb interaction among the carriers [38]. This will further persist during the third stage of the thermalization process and finally results in the formation of a hot FD distribution at $\Delta t \approx 50$ fs.

The signature discriminating the third stage (III) from the other stages is the onset of a net energy drain out of the electron system [decrease of E_{π^*}, see Fig. 3(a)], while the electron distribution is still nonthermal ("nonthermal cooling"). It lasts for ≈ 28 fs until at $\Delta t = 50$ fs the comparison of the experimental data with the calculated results for a FD distribution indicates that finally the electronic system is internally fully thermalized. The energy drain is caused by electron-lattice interaction, which for timescales $\lesssim 500$ fs is dominated by the interaction with SCOPs [22,23]. Notably, during this initial energy relaxation stage the energy drain seems to affect only ΔE_{π^*}, which we associate with the nonthermal component of the electronic excitation, while T_{FD} stays virtually constant at its maximum value of ≈ 5500 K. Figure 3(c) illustrates how this cooling process acts on the electron distribution. The graph displays difference intensities of experimental EDCs and a FD distribution at $T = 5500$ K for different time delays before ($\Delta t = 8$ fs), during ($\Delta t = 22, 36, 50$ fs), and after ($\Delta t = 78$ fs) the nonthermal cooling stage. Whereas the experimental EDCs at $\Delta t = 8$ fs ($T_{\text{FD}} = 3400$ K) and $\Delta t = 78$ fs ($T_{\text{FD}} = 5200$ K) show significant deviations from the FD distribution at $T = 5500$ K over the entire excitation energy regime, the deviations for $\Delta t = 22$ fs and $\Delta t = 36$ fs ($T_{\text{FD}} \approx 5500$ K) are limited to an intermediate energy regime between E_F and $E - E_F \approx 1.3$ eV. The high energy tails of these two EDCs match in contrast the thermalized behavior extremely well. In this part of the electron spectrum thermal equilibrium conditions corresponding to the maximum electron temperature of 5500 K are anticipated already 28 fs before the complete internal thermalization is achieved.

The energy drain by the interaction of the electrons with SCOPs during stage III should affect both the "nonthermal" as well as the "thermal" part of the electron distribution. The internal thermalization of the electron gas promoted by carrier-carrier interaction results, on the other hand, in a net energy transfer from the nonthermal to the thermal part of the electron distribution. The observation of a rigid and thermalized high energy tail during the entire nonthermal cooling stage indicates that the latter process effectively compensates for the energy drain out of the thermal part due to interaction with the lattice.

The final stage of the thermalization process that can be discerned in Fig. 3 (IV, $\Delta t \geq 50$ fs) is characterized by the continuous and simultaneous decrease of E_{π^*} and T_{FD}, with the experimental data following the expectations for a FD distributed electron gas strikingly well. This is indicative for the cooldown of the internally thermalized electron distribution (thermal cooling) due to the interaction with the lattice. This temporal regime was previously studied in detail by various time-domain techniques [9–13,22].

The transition of a photoexcited electron gas in HOPG from a nascent nonthermal towards a thermal distribution is completed within a time period as short as 50 fs. The scenario involves electron-photon, electron-electron, and electron-phonon interaction affecting the response of the system on different timescales. In analyzing the temporal evolution of the excess energy deposited into the electronic system within 7 fs, we were able to experimentally identify characteristic signatures of these interaction processes. Owing to the exceptional time resolution of the trARPES experiment used in the study, we even succeeded in dissecting the complex thermalization process into different stages. The sequence of these stages and the characteristic timescales of energy and momentum exchange among the involved systems are summarized in Fig. 4. For the two fluences investigated in this Letter, no significant differences in the characteristic response times could be observed (see Fig. 4 and Supplemental Material [24]). However, we expect significant changes at substantially lower fluences, particularly as carrier-carrier scattering is very sensitive to the excited carrier density [39]. On the other hand, indirect electronic transitions may become relevant at higher fluences due to saturation effects and Pauli blocking [40]. Moreover, the thermalization of the system can be affected by other experimental parameters, such as bandwidth and photon energy of the applied pump pulses [41]. Similar complex multistep carrier thermalization scenarios are expected also for other materials with reduced screening. The response of these systems to an optical excitation is phenomenologically often described within multitemperature models [42], which
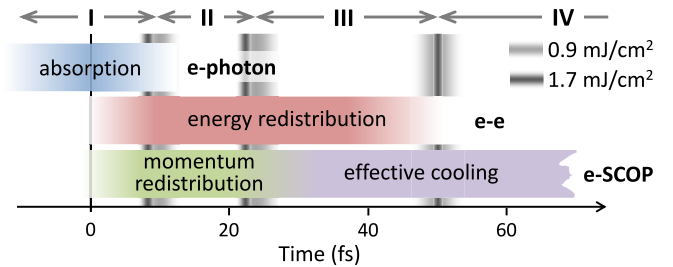

FIG. 4. Stages of thermalization and characteristic timescales of energy and momentum exchange processes. Relevant interaction processes are indicated. Time markers separating the stages result from the evaluation of the experimental data for $F = 0.9$ and $F = 1.7$ mJ/cm^2. Widths of the markers account for the experimental uncertainty.

consider the electronic system being internally thermalized for all times and therefore neglect, for instance, phonon emission during an internal thermalization stage [43]. The method presented here can provide valuable information on the actual state of the electron gas even on the extremely short nonthermal timescales right after excitation.

[*] rohde@physik.uni-kiel.de

[1] T. Winzer and E. Malić, Phys. Rev. B **85**, 241404 (2012).

[2] K. J. Tielrooij, L. Piatkowski, M. Massicotte, A. Woessner, Q. Ma, Y. Lee, K. S. Myhro, C. N. Lau, P. Jarillo-Herrero, N. F. van Hulst, and F. H. L. Koppens, Nat. Nanotechnol. **10**, 437 (2015).

[3] F. Xia, T. Mueller, Y.-M. Lin, A. Valdes-Garcia, and P. Avouris, Nat. Nanotechnol. **4**, 839 (2009).

[4] X. Gan, R.-J. Shiue, Y. Gao, I. Meric, T. F. Heinz, K. Shepard, J. Hone, S. Assefa, and D. Englund, Nat. Photonics **7**, 883 (2013).

[5] V. Ryzhii, M. Ryzhii, A. Satou, T. Otsuji, A. A. Dubinov, and V. Y. Aleshkin, J. Appl. Phys. **106**, 084507 (2009).

[6] H. Karasawa, T. Komori, T. Watanabe, A. Satou, H. Fukidome, M. Suemitsu, V. Ryzhii, and T. Otsuji, J. Infrared, Millimeter, Terahertz Waves **32**, 655 (2011).

[7] Z. Sun, A. G. Rozhin, F. Wang, T. Hasan, D. Popa, W. O'Neill, and A. C. Ferrari, Appl. Phys. Lett. **95**, 253102 (2009).

[8] Z. Sun, T. Hasan, F. Torrisi, D. Popa, G. Privitera, F. Wang, F. Bonaccorso, D. M. Basko, and A. C. Ferrari, ACS Nano **4**, 803 (2010).

[9] K. Seibert, G. C. Cho, W. Kütt, H. Kurz, D. H. Reitze, J. I. Dadap, H. Ahn, M. C. Downer, and A. M. Malvezzi, Phys. Rev. B **42**, 2842 (1990).

[10] J. H. Strait, H. Wang, S. Shivaraman, V. Shields, M. Spencer, and F. Rana, Nano Lett. **11**, 4902 (2011).

[11] S. Winnerl, F. Göttfert, M. Mittendorff, H. Schneider, M. Helm, T. Winzer, E. Malic, A. Knorr, M. Orlita, M. Potemski, M. Sprinkle, C. Berger, and W. A. de Heer, J. Phys. Condens. Matter **25**, 054202 (2013).

[12] J. C. Johannsen, S. Ulstrup, F. Cilento, A. Crepaldi, M. Zacchigna, C. Cacho, I. C. Edmond Turcu, E. Springate, F. Fromm, C. Raidel, T. Seyller, F. Parmigiani, M. Grioni, and P. Hofmann, Phys. Rev. Lett. **111**, 027403 (2013).

[13] A. Stange, C. Sohrt, L. X. Yang, G. Rohde, K. Janssen, P. Hein, L.-P. Oloff, K. Hanff, K. Rossnagel, and M. Bauer, Phys. Rev. B **92**, 184303 (2015).

[14] M. Breusing, C. Ropers, and T. Elsaesser, Phys. Rev. Lett. **102**, 086809 (2009).

[15] D. Brida, A. Tomadin, C. Manzoni, Y. J. Kim, A. Lombardo, S. Milana, R. R. Nair, K. S. Novoselov, A. C. Ferrari, G. Cerullo, and M. Polini, Nat. Commun. **4**, 1987 (2013).

[16] I. Gierz, F. Calegari, S. Aeschlimann, M. Chávez Cervantes, C. Cacho, R. T. Chapman, E. Springate, S. Link, U. Starke, C. R. Ast, and A. Cavalleri, Phys. Rev. Lett. **115**, 086803 (2015).

[17] T. Winzer, A. Knorr, and E. Malic, Nano Lett. **10**, 4839 (2010).

[18] T. Plötzing, T. Winzer, E. Malic, D. Neumaier, A. Knorr, and H. Kurz, Nano Lett. **14**, 5371 (2014).

[19] T. Li, L. Luo, M. Hupalo, J. Zhang, M. C. Tringides, J. Schmalian, and J. Wang, Phys. Rev. Lett. **108**, 167401 (2012).

[20] I. Gierz, M. Mitrano, J. C. Petersen, C. Cacho, I. C. E. Turcu, E. Springate, A. Stöhr, A. Köhler, U. Starke, and A. Cavalleri, J. Phys. Condens. Matter **27**, 164204 (2015).

[21] G. Rohde, A. Hendel, A. Stange, K. Hanff, L.-P. Oloff, L. X. Yang, K. Rossnagel, and M. Bauer, Rev. Sci. Instrum. **87**, 103102 (2016).

[22] T. Kampfrath, L. Perfetti, F. Schapper, C. Frischkorn, and M. Wolf, Phys. Rev. Lett. **95**, 187403 (2005).

[23] H. Wang, J. H. Strait, P. A. George, S. Shivaraman, V. B. Shields, M. Chandrashekhar, J. Hwang, F. Rana, M. G. Spencer, C. S. Ruiz-Vargas, and J. Park, Appl. Phys. Lett. **96**, 081917 (2010).

[24] See Supplemental Material at http://link.aps.org/supplemental/10.1103/PhysRevLett.121.256401 for details on the experimental time resolution, further information on Fig. 3, and time-resolved ARPES data for $F = 0.9$ mJ/cm^2, which includes Ref. [25].

[25] A. Grüneis, C. Attaccalite, A. Rubio, S. L. Molodtsov, D. V. Vyalikh, J. Fink, R. Follath, and T. Pichler, Phys. Status Solidi (b) **245**, 2072 (2008).

[26] I. Gierz, J. Electron Spectrosc. Relat. Phenom. **219**, 53 (2017).

[27] S. Y. Zhou, G.-H. Gweon, J. Graf, A. V. Fedorov, C. D. Spataru, R. D. Diehl, Y. Kopelevich, D.-H. Lee, S. G. Louie, and A. Lanzara, Nat. Phys. **2**, 595 (2006).

[28] A. Grüneis, C. Attaccalite, T. Pichler, V. Zabolotnyy, H. Shiozawa, S. L. Molodtsov, D. Inosov, A. Koitzsch, M. Knupfer, J. Schiessling, R. Follath, R. Weber, P. Rudolf, L. Wirtz, and A. Rubio, Phys. Rev. Lett. **100**, 037601 (2008).

[29] W. S. Fann, R. Storz, H. W. K. Tom, and J. Bokor, Phys. Rev. B **46**, 13592 (1992).

[30] W. S. Fann, R. Storz, H. W. K. Tom, and J. Bokor, Phys. Rev. Lett. **68**, 2834 (1992).

[31] A. Grüneis, R. Saito, G. G. Samsonidze, T. Kimura, M. A. Pimenta, A. Jorio, A. G. Souza Filho, G. Dresselhaus, and M. S. Dresselhaus, Phys. Rev. B **67**, 165402 (2003).

[32] E. Malic, T. Winzer, E. Bobkin, and A. Knorr, Phys. Rev. B **84**, 205406 (2011).

[33] M. Mittendorff, T. Winzer, E. Malic, A. Knorr, C. Berger, W. A. de Heer, H. Schneider, M. Helm, and S. Winnerl, Nano Lett. **14**, 1504 (2014).

[34] E. Malic, T. Winzer, and A. Knorr, Appl. Phys. Lett. **101**, 213110 (2012).

[35] M. Trushin, A. Grupp, G. Soavi, A. Budweg, D. De Fazio, U. Sassi, A. Lombardo, A. C. Ferrari, W. Belzig, A. Leitenstorfer, and D. Brida, Phys. Rev. B **92**, 165429 (2015).

[36] S. Aeschlimann, R. Krause, M. Chávez-Cervantes, H. Bromberger, R. Jago, E. Malić, A. Al-Temimy, C. Coletti, A. Cavalleri, and I. Gierz, Phys. Rev. B **96**, 020301 (2017).

[37] T. Danz, A. Neff, J. H. Gaida, R. Bormann, C. Ropers, and S. Schäfer, Phys. Rev. B **95**, 241412 (2017).

[38] T. Winzer and E. Malic, J. Phys. Condens. Matter **25,** 054201 (2013).

[39] T. Winzer, E. Malić, and A. Knorr, Phys. Rev. B **87,** 165413 (2013).

[40] Y. Yang, G. Kolesov, L. Kocia, and E. J. Heller, Nano Lett. **17,** 6077 (2017).

[41] J. C. König-Otto, M. Mittendorff, T. Winzer, F. Kadi, E. Malic, A. Knorr, C. Berger, W. A. de Heer, A. Pashkin, H. Schneider, M. Helm, and S. Winnerl, Phys. Rev. Lett. **117,** 087401 (2016).

[42] S. I. Anisimov, B. L. Kapeliovich, and T. L. Perel'man, Zh. Éksp. Teor. Fiz. **66**, 776 (1974) [, Sov. Phys. JETP **39**, 375 (1974)].

[43] V. V. Baranov and V. V. Kabanov, Phys. Rev. B **89**, 125102 (2014).